Growth characteristics of glioblastoma spheroids

CHANDRASEKAR NIRMALA[1], JASTI S. RAO[1], ARNOUT C. RUIFROK[2], LAUREN A. LANGFORD[3] and MANDRI OBEYESEKERE[4]

[1]Department of Biomedical and Therapeutic Sciences, College of Medicine at Peoria, University of Illinois, Peoria, IL 61656; [2]Division of Pathology and [3]Laboratory Medicine, [4]Department of Biomathematics, University of Texas M.D. Anderson Cancer Center, 1515 Holcombe Blvd., Houston, TX 77030, USA

Received August 13, 2001; Accepted October 4, 2001

Abstract. Cell spheroids have been proposed as models of early tumor growth from which a better understanding of tumor cell heterogeneity and its effects on treatment response might be gained. Results of experiments performed to understand the underlying dynamics of cell growth within a spheroid formed by SNB19, a high-grade glioblastoma cell line, are presented. We discuss the spatiotemporal distribution of the cells and their cell cycle status based on physical measurements, immunohistochemistry, and flow cytometry analysis. The size of the spheroids and their growth rates were dependent on the initial cell number, the proliferation was mostly limited to the outermost region as the spheroids grew in size, and the number of dead cells increased with age and size as well. Interestingly, though the population of the proliferating cells became localized to the outer rim as spheroids grew, the fraction of proliferating cells did not change drastically. Also, our data reveal that the calculated density varied with respect to age of the spheroid as well as position within the spheroid. We show that a simple exponential model is not adequate for modelling the growth characteristics that have been seen by these experiments. In contradiction to available studies, we report that an acellular (necrotic) center appeared and then disappeared during the period of investigation. Furthermore, after the acellular region disappeared, a few proliferative cells appeared in the center area, raising many questions about the growth-related dynamics of the spheroids formed by this particular cell type.

Introduction

Treatment of tumors is highly complicated because of the heterogeneity in the cell populations. The diverse response of the tumors to therapeutic agents is attributed to the development of resistant cells and capability of the tumor cells to shift between quiescent and proliferating states (1,2). Treatment modalities can be improved only if the growth of these cells is understood, and this is only possible if we have an *in vitro* system that mimics the *in vivo* situation. Spheroids, which can be considered multi-cellular model systems of tissues that are grown with no artificial substrate for cell attachment (3), have been proposed as a model for tumor cell heterogeneity. Spheroids are known to mimic the growth characteristics of tumors (3) and to develop gradients in proliferation with increasing size (4). Studies by Landry *et al* (5) have shown that the regrowth kinetics of cells derived from different regions of multi-cellular spheroids are indeed different. Spheroids provide a system for study of the pre-vascular phase of tumor growth in the absence of tumor-host interactions and for investigating the regulation of growth by three-dimensional cell-cell interactions.

Along with biological experiments to understand the growth dynamics of these spheroids, there have been many attempts to seek a mathematical interpretation of this complex, dynamic system. Many mathematical models have been proposed during the last few decades, ranging from simple Gompertzian models to more extensive, and hence complex, models. These complex models incorporated biological phenomena such as the limitation of proliferation to the outer edge of the spheroid (constant crust models), the emergence and the influence of a necrotic center (inhibitory factors), the availability and transport of nutrients, changing growth status of the cells, and even the possibility of cell migration. Refs. 6-12 detail a few such studies.

Spheroids have been used as *in vitro* experimental models also to study other effects. For example, spheroids have been used to study radiation effects, tumor invasion, and the effects of antisense gene transfer on tumor invasion; some recent refs. are 13-18.

The previous experiments and their models were based on one property of the spheroids, for example, the cell count or the radius with respect to time. None of them had examined how the cells within the spheroids behaved with respect to space and time. A good mathematical model of spheroid growth, however, requires that it accounts for changes in spheroid volume, cell count, distribution of cells within the volume, and the proliferative status of the cells. All of these

Correspondence to: Dr Mandri Obeyesekere, Department of Biomathematics, University of Texas M.D. Anderson Cancer Center, 1515 Holcombe Blvd., Houston, TX 77030, USA
E-mail: mandri@mdanderson.org

Key words: glioblastoma, spheroid model, growth dynamics, necrosis

properties influence the end point results of experimental manipulations of spheroids aimed at understanding tumor growth and invasion. In this study we report the results of experiments that reveal the different dynamics of a glioblastoma spheroid, including all the parameters discussed above.

We conducted experiments on spheroids that were established by a glioblastoma cell line, SNB19, for a duration of 4-5 weeks. Our long-term goal is to derive comprehensive mathematical models that exhibit the spatiotemporal behavior of tumor spheroids. Such models could be used as valuable tools in designing further experiments.

Materials and methods

Spheroid culturing. SNB19 glioblastoma cells were cultured at 37˚C in a 5% carbon dioxide atmosphere in DMEM/F12 medium supplemented with 10% fetal bovine serum. Spheroids were initiated by inoculating $2x10^6$ cells, unless indicated differently, of SNB19 glioblastoma cells in 100-mm dishes containing DMEM/F12 high glucose medium containing 10% fetal bovine serum (FBS) on top of an underlay of 0.75% agar. After 4 days the spheroids were removed, and individual spheroids were placed in a 24-well plate coated with 0.75% agar. The medium was replenished once every other day.

Volume analysis. The size of each spheroid was determined by measuring 2 orthogonal diameters (d1 and d2) on each of the spheroids using an inverted microscope fitted with a calibrated eye piece reticule. The volume (V) was calculated according to the formula: $V = 4/3\pi r^3$, where $r = \frac{1}{2}\sqrt{d1 \cdot d2}$ the geometric mean radius.

Cell counts. Single spheroids were removed, washed with phosphate-buffered saline (PBS), and trypsinized using 0.25% trypsin for 30 min at 37˚C. The trypsin action was stopped by the addition of an equal volume of medium with 10% FBS. The cells were centrifuged and stained with 0.2% trypan blue. The number of live (trypan blue excluding) and dead cells were counted using a hemacytometer under a light microscope.

Flow cytometric analysis. The spheroids were washed with PBS, trypsinized with 0.25% trypsin, and incubated at 37˚C for 30 min. An aliquot containing $0.5x10^6$ cells of each group was pelleted by centrifugation (1200 x g, 5 min), resuspended in PBS, and fixed in 70% ethanol at 4˚C overnight. Fixed cell samples were washed twice with PBS and then resuspended in PBS-Tween containing 50 µg/ml propidium iodide and 100 µg/ml RNase Type I. Stained samples were analyzed for cell cycle phase distribution on a Coulter EPICS XL AB6064 flow cytometer (Beckman Coulter, Fullerton, CA).

Histologic preparation. The spheroids were fixed in 10% formalin and incubated first at 4˚C overnight and then at room temperature for 2-3 days. The material was then embedded in paraffin and sectioned at 5 µm thickness. The sections were stained with hematoxylin and eosin.

MIB-1 immunostaining. Immunohistochemical staining for the MIB-1 antigen was performed using the MIB-1 antibody and the avidin-biotin complex method. Parafffin-embedded tissue sections were deparaffinized and dehydrated. High temperature antigen retrieval was performed in 10 mM sodium citrate, pH 6.0, for 20 min. The slides remained in this solution for 30 min to cool. After a PBS rinse, tissue sections were treated with 0.3% hydrogen peroxide in methanol for 30 min to block endogenous peroxides and then washed in PBS. The slides were transferred to a humid chamber and blocked with normal horse serum in PBS containing 1% bovine serum albumin for 30 min at room temperature. After the overnight incubation with primary antibody at 4˚C, the slides were allowed to warm at room temperature, rinsed in PBS, and placed in antimouse biotinylated antibody for 1 h at 37˚C. After another rinse in PBS, the avidin-biotin complex was applied for 1 h at 37˚C. The slides were developed with 3-amino-9 ethylcarbazole (AEC) and checked under a microscope for adequate color development. The slides were cover slipped with a water-miscible mounting medium after counterstaining with Mayer's hematoxylin.

Optical measurements. Sections of hematoxylin and AEC-stained spheroids were analyzed using the methods described earlier (19). Basically the method consists of the following three steps: i) image acquisition. A Leica DMLB microscope (Leica Microsystems Inc., Deerfield, IL, USA) was equipped with a CCD camera (Hamamatsu, Bridgewater, NJ, USA), interfaced with an IBM computer (International Business Machines Corporation, Armonk, NY, USA) equipped with a Matrox Meteor digitizer board (Matrox Electronic Systems Ltd., Dorval, Quebec, Canada). Light and camera settings were standardized, resulting in average background values of 20±5 (mean ± standard deviation; scale 0-255 from white to black) for the red, green and blue channels. Linearity of the image acquisition setup was tested using a stepped neutral density filter. This was found to be linear with light intensity for all three colors within 2%, over the whole dynamic range of the camera (correlation coefficients of the OD with grayscale values for red, green and blue: $R > 0.996$; $R^2 > 0.993$). The images were captured with a x20 objective lens.

ii) Image processing. The 24-bit RGB images were transferred to a Macintosh G4 (Apple Computer, Cupertino, CA, USA) and processed and analyzed using NIH image version 1.62, developed at the National Institutes of Health (NIH) and available on the Internet from rsb.info.nih.gov/nih-image. Custom macros were written for background correction and transformation from intensity to optical density (OD), to determine the colorvectors for the different stains, for calculation of the color deconvolution matrix, and for the actual color deconvolution of the images. The stored image of an empty field was used for determination of the light entering at each pixel, implicitly correcting for unequal illumination by background subtraction.

iii) Image analysis. The original and OD images were used to generate image masks for determination of overall spheroid area, hematoxylin-positive area, and AEC-positive area. Thresholding of positive and negative areas was performed using minimum error rate classification of foreground and background signal using custom macros. The areas positive

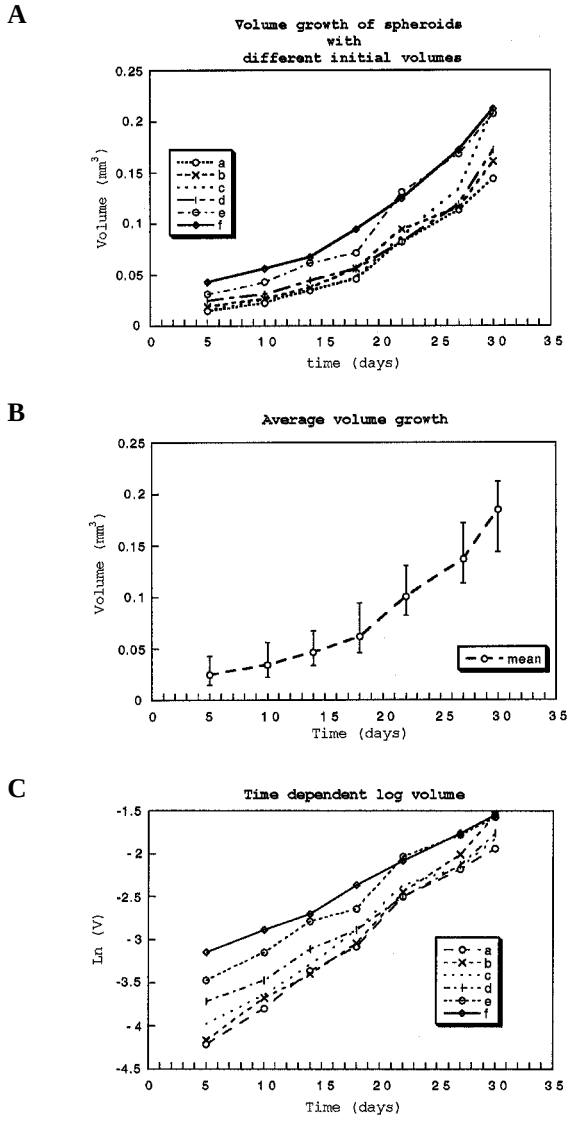

Figure 1. (A), The volume of each spheroid with respect to time. Each spheroid had a different initial volume at day 5. (B), Mean volume of the spheroids of (A) with respect to time (error bars, range of values). (C), The volume on a log scale versus time to investigate the exponential growth rate of the same spheroids that are depicted by (A).

for each stain were measured, and the data were analyzed using standard statistical methods.

Results

Experiment i). Effects of the initial volume on time-dependent volume growth. The volume growth of six spheroids with starting diameters ranging from 380 to 750 μm (spheroids a-f with increasing starting diameter) was studied by measuring the diameter of each, every week for 5 weeks. The size of these spheroids was measured as explained in Materials and methods. The trend of each spheroid's growth was similar for 5 weeks (Fig. 1A). The volume vs. time plot during this time period revealed an approximate exponential growth pattern for every spheroid. In Fig. 1B, the mean volume of these six spheroids with respect to time is presented. Assuming a simple exponential model for the time-dependent volume,

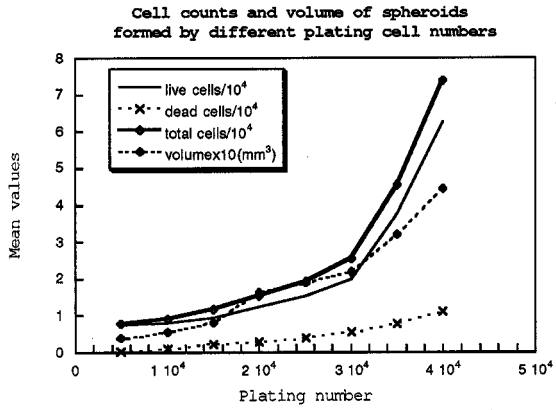

Figure 2. Average live, dead and the total cell numbers and the volume of one week-old spheroids that were formed from differrent plating numbers.

$V(t)$, i.e., $V(t) = V(0)\, e^{\alpha t}$ where t is the time and α is the exponential growth rate of each spheroid, we investigated the dependency of the initial volume V(0) by plotting ln[V(t)] vs. t. As shown by Fig. 1C, the exponential growth rate of each spheroid decreased (the slope of each straight line) with higher initial volume. The starting age of all of these spheroids of different initial volumes was the same.

Experiment ii). Effects of plating different initial cell numbers. Cell numbers ranging from $1x10^4$ to $5x10^4$ cells per well were plated on a 24-well plate coated with 0.75% agar. After 1 week, the diameter of the two largest spheroids formed in each well was measured. Each of these spheroids was trypsinized separately, and the number of dead and live (trypan blue excluding) cells were counted. The volume, the total cell count, and the number of dead cells of these spheroids were directly proportional to the number of cells initially seeded onto the agarose dishes (Fig. 2) (these results are the averages of two spheroids at each plating number).

For the next experiments, spheroids of almost equal size (around 450 μm in diameter), seeded with a constant cell count, were selected and grown in two 24-well plates. Total cell count, number of dead cells (using trypan blue), volume, DNA analysis, and histological studies were performed weekly on a subpopulation of spheroids (five or six) taken from the plates.

Experiment iii). Total cell count, number of dead cells, and volume change with respect to time. Six spheroids were selected every week for a period of 4 weeks to study the volume and cell count changes over time. Diameter measurement and cell counts were done for individual spheroids. The average volume and total cell count showed an exponential growth pattern with respect to time (Fig. 3).

Experiment iv). Cell cycle analysis with respect to time. The percentages of cells in different cell cycle phases with respect to time were determined by flow cytometeric analysis (Fig. 4). With time, the percentage of S+ G2/M-phase cells, the proliferative percentage, decreased slightly. The percentage of

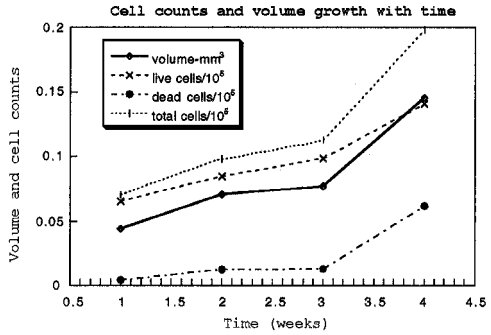

Figure 3. The average cell counts (live, dead and total) and volume of five spheroids at each week.

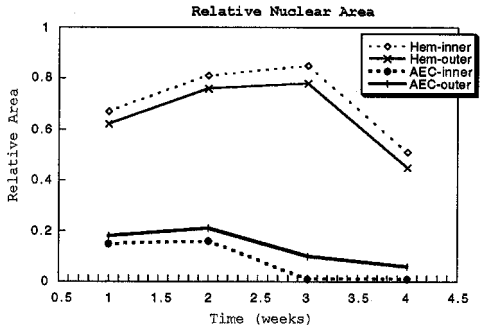

Figure 6. The relative areas stained with hematoxylin (all nuclei) and AEC (MIB-1 positive nuclei) as calculated by image analysis. Data are the average of 3-4 cross sections of spheroids at 1-4 weeks of age.

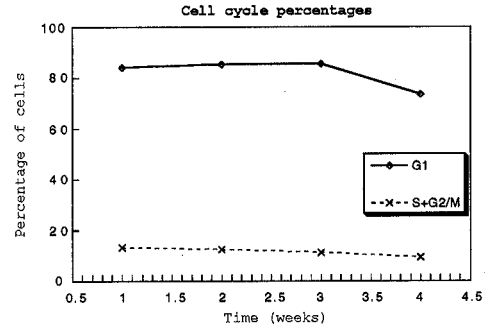

Figure 4. The flow cytometry data of G1-phase and S- and G2/M-phase cell fractions of five spheroids at each time point.

Table I. Relative area in the spheroid center and rim stained by hematoxylin.

Age (weeks)	Center	Rim	Center/Rim
1	0.67±0.11	0.62±0.08	1.09±0.16
2	0.81±0.03	0.76±0.04	1.04±0.03
3	0.85±0.03	0.78±0.05	1.14±0.02
4	0.51±0.11	0.45±0.08	1.14±0.07

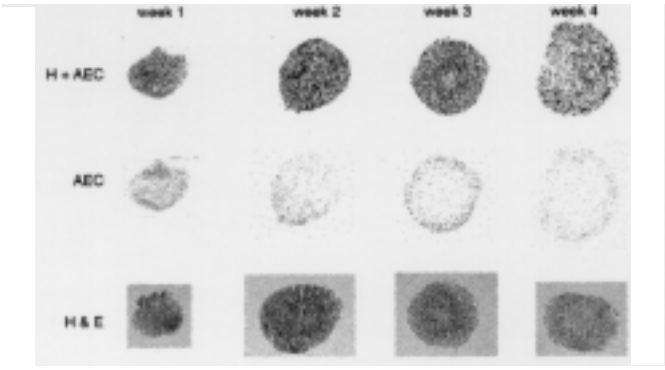

Figure 5. Representative samples of immunohistochemical staining for MIB-1 (row 1 and 2) and hematoxylin-eosin staining of 1-4 week-old spheroids. Row 1, MIB-1 stained with AEC, counterstained with hematoxylin. Row 2, AEC staining only as determined by color-deconvolution of the images of row 1. Row 3, hematoxylin and eosin staining.

G1/G0-phase cells increased very slowly until week 3 and then drastically decreased at week 4.

Experiment v). Light microscopy, spheroid organization with respect to time. The appearance of the spheroids was different under a phase contrast microscope at different weeks. During the first week the cells in the spheroid were less organized, with respect to space, than in the third and fourth weeks. At week 3, the spheroid had a visible, large acellular region that faintly stained with eosin (Fig. 5, first row).

Experiment vi). MIB-1 immunostaining, location of the proliferating cells. This study was undertaken to determine the area of proliferation in the spheroid sections studied in the previous experiment. The MIB-1 mAb labels nuclei in cycling cells. Labeled nuclei were easily identified by visual inspection. During the first 2 weeks of spheroid growth the sections showed more widespread positivity to MIB-1, but during the third and fourth week the staining with MIB-1 was seen more in the outer rim of the spheroid (Fig. 5, second row).

Experiment vii). Distribution of cells within the spheroid. The distribution of MIB-1-positive and -negative cells relative to position in the spheroids was studied using sections obtained from these spheroids at different ages. In Fig. 6 we present the cell density of the center area of half the radius and the outer half-radius rim as revealed by hematoxylin (Hem) and ethylcarbazole (AEC) staining. Cell density was estimated by the relative area occupied by the nuclei. The central-area nuclear density (Hem stain) increased up to a spheroid age of 3 weeks and then decreased. The density in the rim-area was similar, but slightly lower than in the center at all times (Table I). However, the MIB-1 staining (AEC) result was different: the staining seemed to drop after 2 weeks in the center as well as the rim, but more so in the center than in the rim. Therefore, the proliferation in the center seemed to stop after more than 2 weeks (Table II). After 2 weeks, the proliferation in the rim also seemed to decrease, although much less so than in the center, causing the proliferation to

Table II. Relative area stained positive in the spheroid center and rim for MIB-1.

Age (weeks)	Center	Rim	Center/Rim
1	0.15±0.06	0.18±0.07	0.83±0.08
2	0.16±0.10	0.21±0.14	0.70±0.02
3	0.01±0.01	0.10±0.01	0.16±0.07
4	0.01±0.01	0.06±0.03	0.12±0.06

Table III. Fraction of cycling cells in the spheroid center and rim as determined from immunostaining (MIB-1/ hematoxylin).

Age (weeks)	Center	Rim	Center/Rim
1	0.25±0.06	0.34±0.14	0.78±0.19
2	0.18±0.14	0.26±0.20	0.68±0.03
3	0.02±0.01	0.13±0.02	0.14±0.06
4	0.02±0.02	0.13±0.10	0.10±0.05

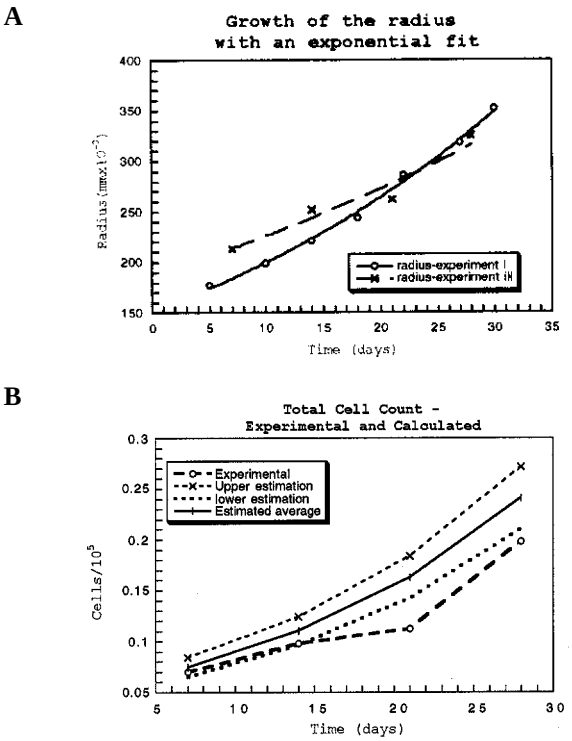

Figure 7. (A), Exponential fits to the radius changes observed in experiments i) and iii). (B), Estimated cell number per spheroid as a function of time assuming constant cell density, compared with experimental data from experiment iii).

be 10 times higher in the rim than in the center at 4 weeks (Table III).

Discussion

Spheroids grown from an established glioma cell line were used to create different microenvironments within an identical cell population. This system is thought to simulate a situation found in underperfused solid tumors where different micro-environments develop as a result of increasing distances from the nourishing capillaries (3). The aim of our study was to see how well spheroids of a clinically highly invasive tumor cell line follow the growth patterns that are established for spheroids of many other cell types and lines. Characteristics of these growth patterns are: i) the volume growth becomes saturated over time; ii) there exists a constant crust of proliferative cells; and iii) the radius of the necrotic center grows with time. As seen in our results, during this time period of investigation, we did not observe a limiting spheroid volume, nor an increasing necrotic central volume with increasing time. Instead, we observed growth of the total volume of the spheroid over time.

The reasons our spheroids did not show a limiting volume growth could be twofold. First, the limits on volume reported in other studies could have been due to depleted growth medium; we replenished ours more often (every other day) than usual. Second, our spheroids could be of an *in vitro* slow-growing cell line compared to the others and we have not continued our experiment long enough to observe such a stabilizing effect. If these are slow-growing, we can assume that these experiments were performed during the early growth time period of these spheroids, before they reached plateau phase. It is well documented in the literature that the early growth phase of most of the spheroids is exponential. Our data from experiments i) and iii) agree well with this concept.

In Fig. 7A we show the exponential fit [$R(t) = R(0)\, e^{\alpha t}$] for the data of time-dependent radius from experiments i) and iii). The best fit for these data are given by $R(t) = 151\, e^{(0.027850)t}$ and $R(t) = 188\, e^{(0.01862)t}$, respectively. The volume growth of these spheroids can be formulated using the radius growth given by the two equations above, assuming the spheroids are spherical. Then the volume doubling time, $T_D (T_D = \frac{\ln 2}{3\alpha})$, for the two cases given by experiments i) and iii) is 8 and 12 days, respectively. If constant cell density is assumed, then the cell doubling time will be the same as volume doubling time. Under this assumption, we can conclude that these spheroids are slow-growing spheroids compared to the spheroids cited in the literature (for example see ref. 20).

Furthermore, these results also show that even for the same batch of spheroids tested under similar conditions, the growth rate α can vary. Hence, a simple exponential growth model as we have used above may not be a sufficient mathematical model.

However, the validity of assuming a constant density is not justified by our data. For example, we can use data from experiment ii) to calculate the cell density in a spheroid of similar size that was used in experiment iii). The average density for the week-old spheroid in the same diameter range is 1.81 (±0.23) $x10^4$ cells/mm^3. For comparison, we show in Fig. 7B the cell counts from experiment iii), the calculated cell counts using the mean density obtained above (mean

density x volume), and the cell counts at the extreme values of the density, the upper and the lower estimates based on the standard deviation of the mean density. This implies that for a long period of time, 4 weeks in this case, volume measurement with the density measured at one time point (at week 1) is not an appropriate method to estimate the total cell count. Hence, the density is not a constant with respect to time. Also from Fig. 6, it is very clear that the cell density is not a constant with respect to time or position. Not the time dependent cell density, total dissociated cell count/total volume for experiment iii) nor the density approximation we obtained by counting the nuclear area on the corresponding sections given by Table I support a constant density. These results suggest cell re-organization in these spheroids during this time period. Furthermore, by both methods of calculating the density, we saw a drop in the cell density at week 4, which implies a reorganization of the glioblastoma cells within these spheroids.

As for the cell cycle status of the cells within the spheroid, our results show a progressive decrease in the proliferative fraction with increasing time. The growth of the spheroids proceeded through various phases. At week 1 we observed that the cells aggregated to initiate the spheroid (closer to a spherical shape), followed by a second week of geometric growth when diffusion of the nutrients is not limiting and almost all the cells are dividing. At the third week, the spheroids increased in size still more (well-formed spherical shapes), with the proliferating area localized to the outer layer and an inner annulus zone of non-proliferative, viable cells, and an acellular inner center considered a necrotic center. By the end of the fourth week, the size of the spheroids increased but without a central core of necrosis. Expression of MIB-1 was diffuse throughout all the layers of the spheroid at week 1, indicating an active proliferative state. But during the third week, the MIB-1 was strongly expressed in the periphery of the spheroid, suggesting it could be the most proliferative compartment in our model. The low level of expression in the center of the spheroid supports a conclusion of no proliferating cells. In the fourth week, along with the disappearance of the necrotic center, strong MIB-1 expression appeared in a very small fraction of cells that occupied the center (data not shown). These results suggest to us that other than the effects due to the diffusion of the nutrients from the exterior some other factors within the spheroid could regulate the growth characteristics in these glioblastoma spheroids.

The spheroid growth models proposed by Freyer and Sutherland (7) and by Freyer (4) assume that growth regulation in spheroids is a competition between stimulatory and inhibitory factors; the relative functions of these factors changes with spheroid growth. Our results also emphasize that the age of the spheroid affects the growth characteristics of these spheroids. Thus it may be improper to interpret results obtained with therapeutic agents restricted to one set of spheriods that are at a fixed size as a general result. This is a major concern, as a majority of the published reports are based on spheriods of the same volume. In our studies we have shown [experiments i) and ii)] how the variability in initial size and plating number affect the growth dynamics of these spheroids.

Also, irrespective of the starting volume of the spheriods, the observed growth differences between the spheroids could be due to the heterogeneity in the subpopulations of cycling (proliferating) versus non-cycling (non-proliferating/quiescent) cells.

We chose 35-day observation period based on the literature, which generally found that spheroids reached plateau phase in 8-25 days. The volumes of the spheroids that had different initial volumes in experiment i), however, would approach a single value (volume) at around day 41. This value can be derived by extrapolating the graphs shown in Fig. 1C. Future research on these types of spheroids should thus run beyond 41 days to observe the critical outcome.

In terms of modeling the growth of these spheroids, we conclude that neither the volume growth nor the cell count of spheroids of this type can be modeled by a simple exponential formula. A proper simulation will have to incorporate spatio-temporal changes, including those that have been reported here. Hence, we need to model the growth of these spheroids by more complex mathematical formulations. The simulation of the volume growth of these spheroids by a Gompertzian function is still to be investigated.

Results from these experiments suggest that some growth properties of the tumor spheroids formed by SNB19 are similar to those already known for other spheroids, e.g., volume growth and proliferative rim development. However, the appearance and disappearance of the necrotic center and the non-limiting volume growth for this length of time have not been reported in other studies. It has been reported that the activation of a poly(ADP-ribose) polymerase (PARP) is a potential candidate for the regulation of necrosis in glioblastoma (21). It would be interesting to study the expression of PARP in these glioblastoma spheroids at different weeks of growth. In a previous study by Weiss (22) the cells nearer to the necrotic cells showed a greater detachment than from other areas of the tumor. This could be due to the release of materials, for example, lysosomal enzymes, from the cells during necrosis (23). Earlier reports have shown the induction of growth factors in response to hypoxia in the central zone (24). This implies that repopulation could be due to the induction of growth factors at the zone of necrosis. Whether these processes contribute to the disappearance of the acellular region we observed is still to be investigated. We found the acellular region to be repopulated with cells, and a few of them were proliferative at week 4. Based only on these two findings, it is difficult to conclude what type of a reorganization took place for the acellular region to be repopulated. Whether cells moved from the surrounding annulus region to the center or whether the live cells in the annulus proliferated rapidly during this time period to repopulate the center is a question. Since we observed a reduction of the cell density in the center from week 3 to 4, and most of the cells were live but not proliferative at week 4, the latter concept is not well supported.

Our result, disappearance of an acellular region, could be specific to this specific glioblastoma cell line. If so, we are faced with many questions. Among them are, when do spheroids of this type start showing a necrotic center? Does the necrotic area disappear due to reorganization and if so, when does this happen? Do the cells in the dormant (G0-phase) rim move into the necrotic area? Will the necrotic center reappear if the spheroid is kept growing for a few more weeks? Therefore, further studies on these spheroids

are needed to understand the different biological processes that control the dynamics of the growth of these particular spheroids. Such an understanding is crucial for developing a reliable mathematical model for the growth of these tumor spheroids. Furthermore, spheroid-based studies of the effects of treatment could produce variable results based on the size and age of the spheroid. So, an in depth understanding of the growth of these spheroids is critical to our ability to produce valid comparisons of chemotherapeutic agents and radiotherapeutic regimens applied to spheroids.

Acknowledgements

This work was supported in part by NIH/NIGMS-GM59918 (to M.N.O.) and by CA-75557 (to J.S.R.).

References

1. Potmesil M and Goldfeder A: Cell cycle kinetics of irradiated tumors: cell transition from the non-proliferating to the proliferating pool. Cell Tissue Kinet 13: 563-570, 1980.
2. Kallman RF, Combs CA, Franko AJ, Furlong BM, Kelley SD, Kemper HL, Miller RG, Rapacchietta D, Schoenfeld D and Takahashi M: Evidence for the recruitment of non-cycling clonogenic tumor cells. In: Radiation Biology in Cancer Research. Meyn RE and Withers HR (eds). Raven Press, New York, pp397-414, 1980.
3. Sutherland M: Cell and environment interactions in tumor microregions: the multicell spheroid model. Science 240: 177-184, 1988.
4. Freyer JP: Role of necrosis in regulating the growth saturation of multicellular spheroids. Cancer Res 48: 2432-2439, 1988.
5. Landry J, Freyer JP and Sutherland RM: A model for the growth of multicell tumor spheroids. Cell Tissue Kinet 15: 585-594, 1982.
6. Conger AD and Ziskin MC: Growth of mammalian multicellular tumor spheroids. Cancer Res 43: 556-560, 1983.
7. Freyer JP and Sutherland RM: Regulation of growth saturation and development of necrosis in EMT6/Ro multicellular spheroids by the glucose and oxygen supply. Cancer Res 46: 3504-3512, 1986.
8. Marusic M, Bajzer Z and Vuk-Pavlovic S: Tumor growth *in vivo* and as multicellular spheroids compared by mathematical models. Bull Math Biol 56: 617-631, 1994.
9. Groebe K and Mueller-Klieser W: On the relation between size of necrosis and diameter of tumor spheroids. Int J Radiat Oncol Biol Phys 34: 395-401, 1996.
10. Pettet GJ: The migration of cells in multicell tumor spheriods. Bull Math Biol 63: 231-257, 2001.
11. Freyer JP and Schor PL: Regrowth kinetics of cells from different regions of multicellular spheroids of four cell lines. J. Cell Physiol 138: 384-392, 1989.
12. Chignola R, Schenetti A, Chiesa R, Foroni R, Sartoris S, Brendola A, Tridente G, Andrighetto G and Liberati D: Oscillating growth patterns of muticellular tumour spheroids. Cell Prolif 32: 39-48, 1999.
13. Kondraganti S, Mohanam S, Chintala SK, Kin Y, Nirmala C, Lakka SS, Adachi Y, Kyritsis AP, Ali-Osman F, Sawaya R, Fuller GN and Rao JS: Selective suppression of matrix metalloproteinase-9 in human glioblastoma cells by antisense gene transfer impairs glioblastoma cell invasion. Cancer Res 60: 6851-6855, 2000.
14. Mohanam S, Jasti SL, Kondraganti S, Chandrasekar N, Lakka SS, Kin Y, Fuller GN, Yung AWK, Kyritsis AP, Dinh DH, Olivero WC, Gujarati M, Ali-Osman F and Rao JS: Down-regulation of cathepsin B expression impairs the invasive and tumorigenic potential of human glioblastoma cells. Oncogene 20: 3665-3673, 2001.
15. Santini MT and Rainaldi G: Multicellular tumour spheroids in radiation biology. Int J Radiat Biol 75: 787-799, 1999.
16. Koshyomn S, Penar PL, McBride WJ and Taatjes DJ: Four-dimensional analysis of human brain tumor spheroid invasion into fetal rat brain aggregates using confocal scanning laser microscopy. J Neurooncol 38: 1-10, 1998.
17. Nygaard SJ, Haugland HK, Laerum OD, Lund-Johansen M, Bjerkvig R and Tysnes OB: Dynamic determination of human glioma invasion *in vitro*. J Neurosurg 89: 441-447, 1998.
18. Cho KK, Mikkelsen T, Lee YJ, Jiang F, Chopp M and Rosenblum ML: the role of protein kinase C alpha in U-87 glioma invasion. Int J Dev Neurosci 17: 447-461, 1999.
19. Ruifrok A and Johnston D: Quantification of immunohistochemical staining by colour deconvolution. Anal Quant Cytol Histol (In press).
20. Durand RE: Multicell spheroids as a model for cell kinetic studies. Cell Tissue Kinet 23: 141-159, 1990.
21. Wharton SB, McNelis U, Bell HS and Whittle IR: Expression of poly(ADP-ribose) polymerase and distribution of poly(ADP-ribosyl)ation in glioblastoma and in a glioma multicellular tumor spheroid model. Neuropathol Appl Neurobiol 26: 528-535, 2000.
22. Weiss L: Tumor necrosis and cell detachment. Int J Cancer 20: 87-92, 1977.
23. Turner GA and Weiss L: Some effects of products from necrotic regions of tumors on the *in vitro* migration of cancer and peritoneal exudate cells. Int J Cancer 26: 247-254, 1980.
24. Schweiki D, Neeman M, Itin A and Keshet E: Induction of vascular endothelial growth factor expression by hypoxia and by glucose deficiency in multicell spheroids: implications for tumor angiogenesis. Proc Natl Acad Sci USA 31: 768-772, 1995.